Development of Feature Extraction Using High-Resolution RGB Images and Homography Transformation to Inspect RC Walls Rebar Works

Young-Gun Baek[1], Rong-Lu Hong[1], Il-Gyo Choi[2], Kyung-Ho Lee[1], Ju-Hyung Kim[1]

[1] Department of Architectural Engineering, Hanyang University, Seoul, Republic of Korea
[2]ON Construction Co., Ltd., Yeongdeungpo-gu, Seoul, Republic of Korea
byggun456@naver.com, abraham0814@hanyang.ac.kr, jupi0515@hanmail.net, mbl00@naver.com, kcr97jhk@hanyang.ac.kr

Abstract –

Reinforcing bars (rebars) are essential for resisting tensile forces and ensuring structural safety in reinforced concrete systems. However, current rebar inspection practices rely on manual and sampling-based measurements, leading to human errors and limiting inspection coverage. Although automated 3D and LiDAR-based inspection systems have been explored, their adoption rate remains low due to high cost and workflow complexity. To address these challenges, this study presents a cost-efficient vision-based inspection framework that combines high-resolution image analysis and marker-assisted geometric correction. The proposed method detects rebar and marker regions in low-resolution images, refines intersection keypoints in high resolution, performs marker-based rectification, and computes rebar spacing, diameter, and quantity from the corrected geometry. Experiments under varied distances and viewing angles demonstrated accurate and reliable performance, achieving 100% accuracy in counting vertical and horizontal rebars, mean absolute errors of 0.59 mm for diameter and 4.05 mm for spacing. These results confirm practical, low-cost automated rebar measurements for construction inspection.

Keywords –

Reinforcing bar; Convolutional Neural Network; Homography Transformation

1 Introduction

Quality control in the construction industry is a fundamental process for securing the structural safety of buildings. In particular, reinforcing bars (rebars) are primary load-bearing components that resist tensile forces in reinforced concrete members; therefore, improper placement of rebar can lead to serious defects such as cracking or corrosion [1,2]. Accordingly, accurate inspection of the number, diameter, spacing, and position of rebars before concrete casting is critical to ensure structural safety and construction quality [3]. However, conventional rebar inspection still depends on manual measurement and visual inspection, which are time-consuming and prone to human errors [4]. Specifically, of wall reinforcement, the bars are densely arranged and extend across a large area, which increases the amount of inspection work and makes the process highly labor-intensive. For these reasons, automation and systematization of rebar inspection processes is urgently needed to improve inspection efficiency and reliability[4].

Previous studies primarily rely on LiDAR-based 3D point cloud models to measure rebar diameter, quantity, and spacing [5–6]. Although laser-scanning-based approaches provide high accuracy, their applicability to real-time field inspection is limited due to the high equipment cost and the heavy computational burden [4,7]. As a cost-effective alternative to laser scanners, research has progressed to inspect rebars based on image processing and deep learning on RGB images [8,9]. This is mainly due to the widespread availability, low hardware cost, and ease of deployment of RGB cameras. However, these methods require an orthogonal camera angle, thereby limiting their applicability in dynamic construction environments. Photogrammetry-based 3D reconstruction has also been explored, but this approach typically requires a large number of images for a single rebar segment and involves long processing times, limiting its feasibility for on-site use [7]. Depth cameras have been frequently employed in rebar inspection studies, providing guaranteed measurement accuracy as laser scanners [1,10]. However, the accuracy of depth cameras decreases as the distance from the rebar increases and is further reduced as the camera angle deviates from the orthogonal condition to the rebar mat [5,10]. While these limitations may not be significant for small areas or short measurement ranges, they cause the inspection process to become inefficient when applied to extensive wall reinforcement. Furthermore, the spatial complexity and tight schedules of construction sites hinder the ability to maintain a fixed camera angle.

To overcome these challenges, this study introduces a low-cost rebar placement quality inspection method based on a high-resolution DSLR (digital single-lens reflect) camera with marker-based calibration [11]. The high-resolution DSLR camera ensures the acquisition of necessary pixel density for the precise extraction of fine rebar features, even from long distances. Compared to LiDAR systems, the high-resolution DSLR camera is highly cost-effective and easy to maintain, thus securing high field applicability. Moreover, markers enable the compensation of perspective distortion through homography transformation and serve as a reference for converting pixel units into actual distances [12].

However, even with high-resolution images, extracting fine rebar features from long distances remains challenging. Traditional image processing techniques are susceptible to lighting variations, shadows, complex backgrounds, and noise, which hinder reliable detection in real-world construction environments [10]. Meanwhile, convolutional neural network (CNN)–based methods provide strong detection performance across various environments, but the computational cost increases significantly when processing high-resolution images, which limits real-time applicability [13]. Most CNN-based studies mitigate this computational burden using downsampling, but this leads to the loss of fine visual details and degrades measurement accuracy [8,9,12]. Because rebars are thin, small objects, their pixel footprint becomes extremely limited at long distances, and downsampling further reduces available information, increasing the likelihood of detection and measurement failure.

To address these limitations, the proposed method does not directly apply a CNN to the entire high-resolution image [11]. Instead, it restructures the role of CNNs by decomposing the analysis into two resolution-specific stages. At the low-resolution stage, a CNN is employed solely for global scene understanding and candidate localization, identifying rebar intersection regions and markers with minimal computational cost. These coarse predictions are not used for measurement but only to determine where high-resolution analysis is necessary. Subsequently, only the selected regions of interest are reprojected into the original high-resolution image and processed by a dedicated high-resolution network for metric-level localization. Through this resolution-aware role separation, the proposed method preserves fine geometric details required for accurate rebar measurement while avoiding the prohibitive computational cost of processing the entire image at high resolution [11].

The proposed method detects rebar intersection regions and markers from low-resolution images through a Dual-head Faster R-CNN and then processes the corresponding high-resolution patches with a modified High-Resolution Network (HRNet) to extract precise coordinates of rebar intersections. Subsequently, homography transformation is performed with the marker corner points as the reference frame to provide a perspective-corrected image and to compute the rebar count, diameter, and spacing. Through this process, the proposed method preserves detailed high-resolution information while minimizing computational cost, enabling efficient and accurate rebar inspection even at long distances and under various camera angles.

2 The Proposed Method

2.1 Overview of the Proposed Framework

This study proposes a method for the automated extraction of rebar count, diameter, and spacing in dense and extensive wall reinforcement structures using high-resolution images and fiducial markers. The overall procedure consists of four stages [11]. First, the entire input image is processed by a Dual-head Faster R-CNN to detect markers and rebar cross-section regions. For computational efficiency, the input image is scaled down to 600×400 pixels. The model is designed with a single backbone and two separate heads: one to predict markers in the form of bounding boxes and the other to predict rebar cross-section regions in the form of keypoints. This architecture enables the efficient extraction of necessary Regions of Interest (ROIs) even from noisy field images. Second, the detected rebar cross-section ROIs are projected onto the original high-resolution image, cropped to 256×256 pixels, and input into modified HRNet. Since modified HRNet maintains high-resolution representations for feature extraction, it can reliably estimate the four coordinates of the rebar corner points, even when captured from a long distance or against a complex background. Third, a Homography transformation is performed based on the marker's corner points to generate a perspective-corrected image. This transformation achieves perspective correction in non-frontal shooting environments and computes the pixel-to-real distance scale factor using the marker’s known dimensions. Finally, the rebar diameter is calculated from the distances between the four corner points, while the rebar spacing is derived from the distances between centroids, defined as the intersection points of the diagonals formed by those corner points. The overview of the proposed method is shown in Figure 1.

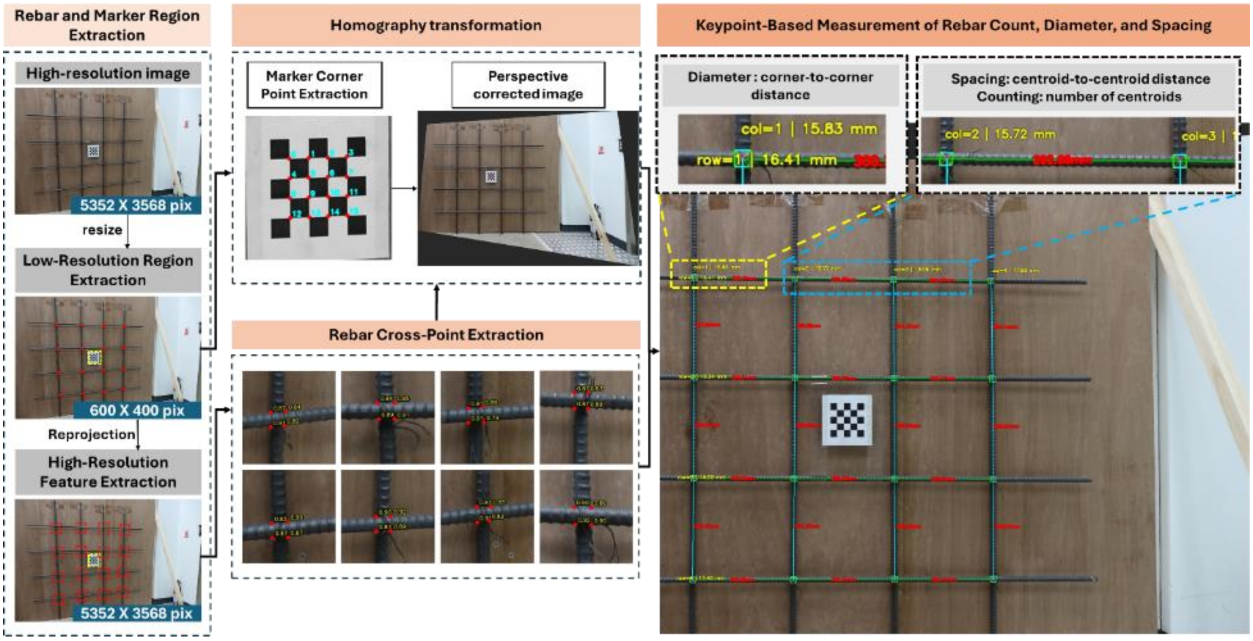

Figure 1. Overview of the proposed method

2.2 Dual-head Faster R-CNN for Rebar and Marker Detection

Since directly processing high-resolution images incurs a significant computational and memory burden, the proposed method first detects ROIs at a low-resolution stage and then performs precise keypoint extraction on the corresponding high-resolution patches. We designed a Dual-head Faster R-CNN with a single backbone and two heads to detect the ROIs from the low-resolution input image [11]. The model architecture shown in Figure 2. The Detector Head, which maintains the structure of the conventional Faster R-CNN, is designed to detect markers as bounding boxes, thereby filtering background and noise when the corner points are subsequently extracted. The Point Heatmap Head is an added component that performs convolutional operations directly on the feature maps extracted from the Feature Pyramid Network (FPN) to generate a heatmap, ensuring stable detection of the rebar keypoints. This architecture is designed to efficiently extract only the necessary ROIs even from noisy field images.

2.2.1 Experimental Settings of Dual-head Faster R-CNN

A dataset of 500 high-resolution rebar and marker images, resized to 600×400 pixels, was collected in a laboratory setting. Data augmentation (flips, blurring,

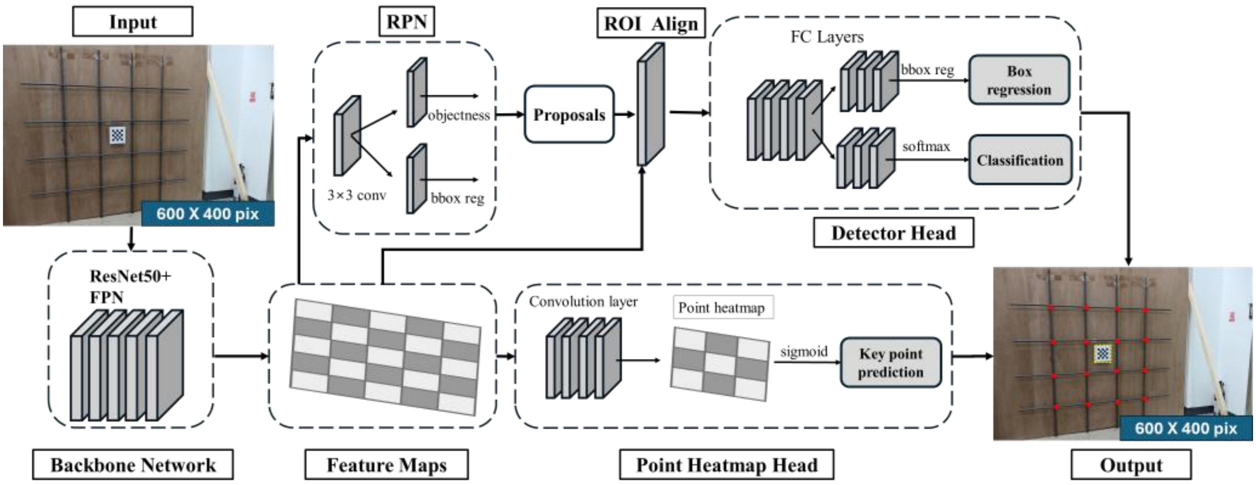

Figure 2. Architecture of the Dual-head Faster R-CNN

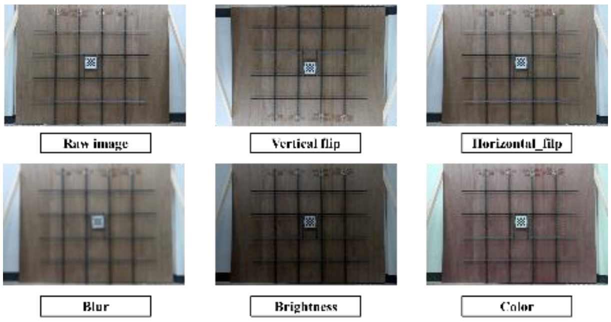

Figure 3 . Examples of data augmentation for Dual-head Faster R-CNN

brightness, color adjustments) expanded the final dataset training, 10% for validation, and 10% for testing. Examples of data augmentation are illustrated in Figure 3. Label consistency was preserved by applying identical geometric transformations to both images and annotations. The model introduced a Dual-head Faster R-CNN with a ResNet-50 FPN backbone, initialized using ImageNet pre-trained weights to leverage transfer learning for fast and stable convergence. Optimization was performed using SGD with a Cosine Annealing with Warm Restarts scheduler, a batch size of 2, and 70 epochs with early stopping. The total loss is the weighted sum of the standard Detection Loss (L_{det}) and a BCEWithLogits-based Heatmap Loss (L_{hm}), defined as:

$$L_{total} = L_{det} + w \cdot L_{hm} \tag{1}$$

Where w is the weight coefficient for the Heatmap Loss which was set to 1.8. The evaluation of bounding boxes was performed using standard metrics, including AP50, AP75, and mIoU. The evaluation of keypoint estimation was performed using the Percentage of Correct Keypoints (PCK) metric with pixel radius thresholds of 2, 5, and 8 (PCK@2, PCK@5, and PCK@8). which is computed as:

$$PCK@\rho = \frac{N_{correct}(\rho)}{N_{gt}} \tag{2}$$

$N_{\mathrm{correct}}(\rho)$denotes the number of predicted keypoints within a pixel distance threshold ρ from the ground truth, and N_{gt} represents the total number of ground-truth keypoints.

2.3 Modified HRNet for Keypoint Extraction

Although initial rebar intersection points are detected at low resolution using a Dual-head Faster R-CNN, their direct reprojection to the high-resolution image is insufficient for precise localization due to pixel-level inaccuracies. Therefore, this study employs a high-resolution patch-based refinement approach using HRNet [11]. Accordingly, high-resolution patches of 256×256 pixels are cropped around the intersection point coordinates predicted by the dual-head Faster R-CNN, and the four corner vertices of the intersection region are precisely estimated using the modified HRNet. Figure 4 presents the architecture of the modified HRNet. To reduce computational overhead, deeper stages of the original HRNet that are unnecessary for precise keypoint estimation on small image patches are omitted. In addition, HRNet integrates a high-resolution feature stream with parallel lower-resolution branches through multi-resolution fusion. Furthermore, adopting a keypoint-based approach simplifies the model structure and reduces computational costs, as it estimates only the minimum required coordinates without predicting the entire pixel area, unlike bounding-box- or mask-based methods. Through this patch-based refinement process, high-resolution rebar features can be extracted with substantially reduced computational cost, as the network operates only on localized regions instead of processing the entire high-resolution image.

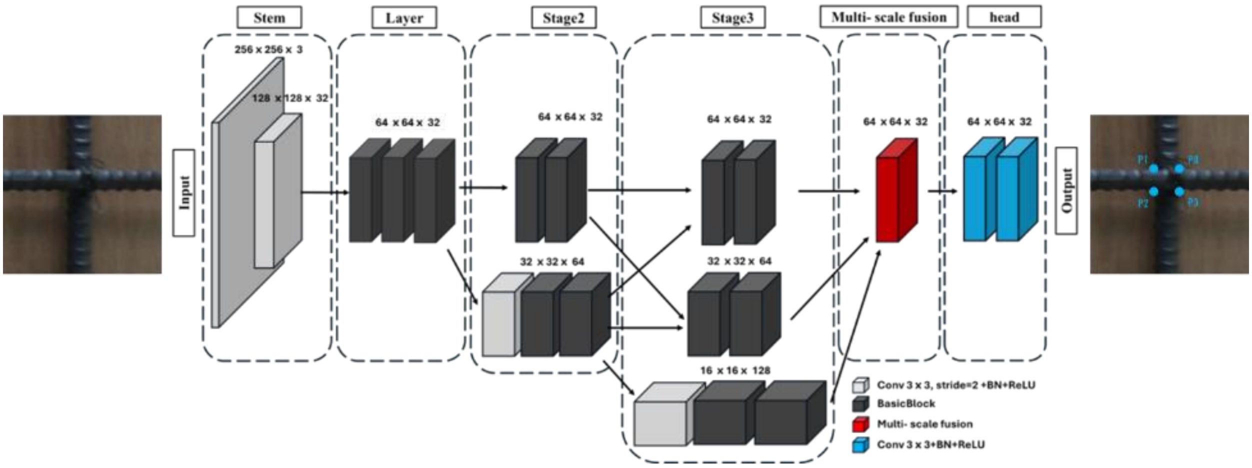

Figure 4. Architecture of the modified HRNet

2.3.1 Experimental Settings of Modified HRNet

The dataset for training modified HRNet was constructed from 880 image patches of size 256×256 pixels, cropped around the rebar intersection centers predicted by the dual-head Faster R-CNN. Extensive data augmentation was applied, including horizontal flips, rotation, blurring, and brightness and color adjustments. Examples of data augmentation are illustrated in Figure 5. The dataset was split into 80% for training, 10% for validation, and 10% for testing. Modified HRNet was trained using the AdamW optimizer, and a batch size of 5, for a maximum of 100 epochs. Early stopping was applied with a patience of 15 epochs, and no transfer learning was employed. The loss function was defined as the mean squared error (MSE) between the predicted heatmaps and the corresponding ground-truth heatmaps, computed using the batch-averaged loss to improve training stability. Keypoint estimation performance was evaluated using the PCK metric at pixel radius thresholds of 2, 5, and 8 (PCK@2, PCK@5, and PCK@8).

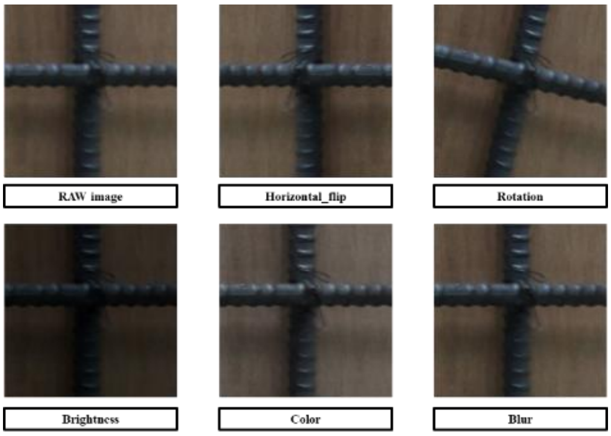

Figure 5. Examples of data augmentation for Modified HRNet

2.4 Geometric Feature Based Rebar Inspection and Quantification

2.4.1 Homography Transformation

In this study, rebar diameter and spacing were quantitatively extracted by combining high-resolution rebar intersection point coordinates with chessboard marker-based geometric correction. To ensure stable corner detection under long-distance imaging conditions, 5×5 chessboard markers with a side length of 20 mm were employed. The marker bounding boxes, detected by the Dual-head Faster R-CNN, were mapped onto the original high-resolution image, and their corner points were precisely extracted using the findChessboardCorners function of OpenCV. The detected marker corner points were matched with their corresponding reference points defined on a marker-aligned virtual planar grid to estimate the homography matrix H. The estimated transformation was then applied to the input image as well as to the rebar corner coordinates estimated by HRNet, enabling rebar measurements to be conducted in a common, perspective-corrected system. Figure 6 illustrates an example of the perspective-corrected image generated using the marker-based homography.

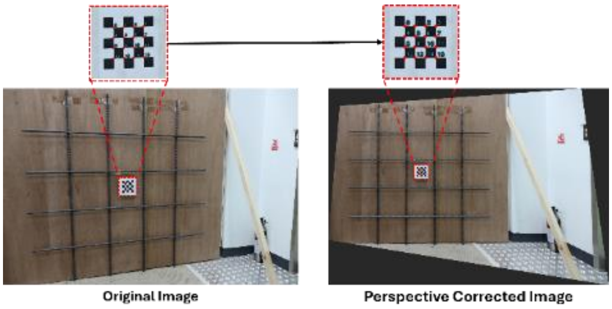

Figure 6. Perspective-corrected image using marker-based Homography Transformation

2.4.2 Rebar Diameter Calculation

In this study, the rebar diameter is estimated from the distances between four corner coordinates predicted by HRNet on a perspective-corrected image obtained via marker-based homography. The pixel distances are subsequently converted to real-world units using a scale factor derived from the known geometry of the marker. To ensure consistent point ordering across samples, the top-right point in the image coordinate system is selected as the reference point ($P1$), and the remaining points are arranged in a counterclockwise order as $P2$, $P3$, and $P4$. Based on the resulting quadrilateral, opposing sides are paired and their average lengths are computed. Here, Length A corresponds to the vertical rebar direction, while Length B represents the horizontal rebar direction. Figure 7, rebar diameter estimation is performed on the perspective-corrected image by measuring the distances between HRNet-detected corner points and converting them into real-world units using the marker-based scale factor. Finally, the estimated diameters for the vertical and horizontal rebars are stored separately according to the row and column indices defined during the spacing extraction process.

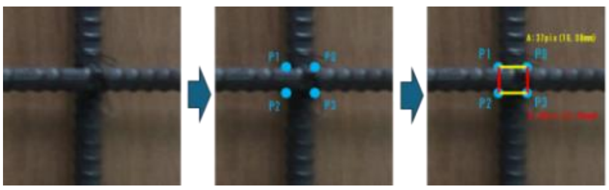

Figure 7. Rebar diameter estimation

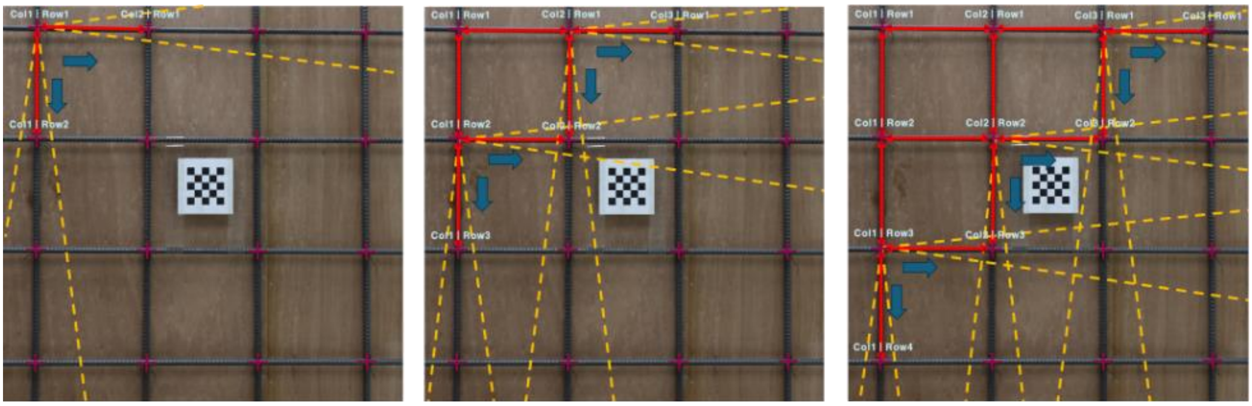

Figure 8. Grid recognition and spacing extraction based on rebar centroids

2.4.3 Calculation of Rebar Spacing and Count

In this study, the centroid of each rebar cross-section is defined as the intersection point of the diagonals $\overline{P1P3}$ and $\overline{P2P4}$ computed from the four corner coordinates estimated by HRNet. These centroids collectively form a grid-like pattern across the image, and their relative spatial arrangement is used to extract rebar spacing. To establish the grid structure, the centroid located at the top-left position in the image coordinate system is selected as the reference point. From this reference, the spacing search is sequentially expanded in the horizontal and vertical directions. An angular tolerance of 30° is applied during the search to accommodate geometric distortions caused by construction tolerances and variations in camera viewpoint. Each detected centroid is then assigned a unique column (col) and row (row) index based on its relative horizontal and vertical displacement from the reference centroid. During this indexing process, the spacing between adjacent centroids is simultaneously computed. By enforcing consistent directionality and angular tolerance, this grid-based strategy is designed to remain effective even under non-uniform rebar layouts or partially missing intersections, which are commonly encountered in real construction environments. Figure 8 illustrates the grid recognition procedure. The yellow lines indicate the 30° angular tolerance used during centroid association, while the red arrows represent the recognized spacing between adjacent centroids. The figure also visualizes the sequential assignment of row and column indices as each centroid is identified.

3 Results and Discussion

3.1 Experimental Setup

Image data were acquired using an 18-megapixel Canon EOS 100D DSLR camera, and a total of 500 images containing rebars and fiducial markers were collected in a controlled laboratory environment. The experiment was conducted in a controlled laboratory environment designed to reflect practical wall reinforcement conditions. Four D16 rebars, each 1.5 m in length, were arranged on a veneer plywood in a 3 × 3 grid pattern with a spacing of 300 mm, and fiducial markers were installed parallel to the rebars. The ground-truth rebar spacing was measured using a tape measure for quantitative comparison with the estimated results.

For image acquisition, the shooting distance was varied from 2.0 m to 4.0 m at intervals of 0.5 m to evaluate the effect of increasing distance and associated focus degradation on measurement accuracy. At each distance, more than 30 images were captured under free-view (non-frontal) perspectives. The marker-based configuration also enabled the estimation of camera extrinsic parameters, allowing the influence of viewpoint variations on image projection and measurement accuracy to be analyzed. Model performance was evaluated using the Mean Absolute Error (MAE) and the Mean Relative Error (MRE).

3.2 Detection and Refinement Model Evaluation

3.2.1 Performance of Dual-head Faster R-CNN

The Dual-head Faster R-CNN achieved optimal performance at the 68th epoch, yielding AP50 = 1.0000, AP75 = 1.0000, mIoU = 0.9633, and PCK@8/5/2 of 0.9990/0.9901/0.5315. Detailed results are summarized in Table 1.

Table 1. Evaluation metrics of Dual-head Faster R-CNN

Marker Detection		Rebar Detection	
AP50	1.0000	PCK@8	0.9992
AP75	1.0000	PCK@5	0.9901
mIoU	0.9633	PCK@2	0.5315

3.2.2 Performance of M~~m~~odified HRNet

In the training of modified HRNet, early stopping with a patience of 15 epochs was applied and triggered at epoch 71. Evaluation on an independent test dataset yielded PCK@8/5/2 of 0.9980/0.9957/0.8930. Table 2 summarizes the prediction performance of the HRNet model.

Table 2 Evaluation metrics of modified HRNet

Evaluation index	Result
PCK@8	0.9980
PCK@5	0.9957
PCK@2	0.8930

3.3 Rebar Quantification Results

3.3.1 Rebar Counting Results

The proposed method was evaluated under varying distances (2.0–4.0 m) and viewpoints. Under all tested conditions, the numbers of both vertical and horizontal rebars were correctly estimated with 100% accuracy. These results demonstrate the robustness and practical applicability of the proposed method in real-world field environments.

3.3.2 Rebar Diameter Measurement Results

The results of rebar diameter estimation show that the MAE remained within 0.50–0.59 mm (3.1–3.7%) up to 3.5 m, increasing to 0.77 mm at 4.0 m. This trend is consistent with the reduction in effective pixel resolution as the camera-to-object distance increases, which limits localization precision. The results are summarized in Table 3.

Table 3. Rebar diameter accuracy at different distances

Distance	MAE (mm)	MRE (%)
2.0 m	0.5859	3.7045
2.5 m	0.5100	3.3702
3.0 m	0.5009	3.1310
3.5 m	0.5788	3.5556
4.0 m	0.7747	4.8427

The effect of the viewing angle on rebar spacing estimation was evaluated. The MAE increased from 0.51 mm to 0.86 mm, while the corresponding error rate rose from 3.20% to 5.40% as the viewing angle increased. This behaviour is explained by the fact that, although homography-based planar correction mitigates perspective distortion, residual errors arise at larger view angles due to the three-dimensional geometry of the rebars. A summary of the results is provided in Table 4.

Table 4. Rebar diameter accuracy at different angles

Angle	MAE (mm)	MRE (%)
0-10°	0.5127	3.2045
10-20°	0.5788	3.6178
20-30°	0.6209	3.8808
≤ 30°	0.8642	5.4012

3.3.3 Rebar Spacing Measurement Results

The results of rebar spacing estimation show that the MAE remained within 3.6–4.1 mm (1.2–1.4%) up to 3.5 m, increasing to 4.65 mm (1.55%) at 4.0 m. This trend is consistent with the reduction in effective image resolution at longer distances, which limits the precision of marker feature point localization. The quantitative results are summarized in Table 5.

Table 5. Rebar spacing accuracy at different distances

Distance	MAE (mm)	MRE (%)
2.0 m	3.9208	1.3060
2.5 m	3.6027	1.2061
3.0 m	4.0948	1.3641
3.5 m	3.9787	1.3253
4.0 m	4.6484	1.5487

The effect of the viewing angle on rebar spacing estimation was analyzed, with the MAE ranging from 3.8 mm to 4.5 mm and the corresponding error rates between 1.2% and 1.5%, showing a gradual increase as the viewing angle increased. In particular, an increase in error was observed for viewing angles exceeding 30°. This behavior is attributed to the fact that, although marker-based planar correction mitigates perspective distortion, residual errors arise at larger view angles due to the three-dimensional geometry of the rebars, which is consistent with the trends observed in diameter estimation. The results are summarized in Table 6.

Table 6. Rebar spacing accuracy at different angles

Angle	MAE (mm)	MRE (%)
0-10°	3.8600	1.2858
10-20°	4.1303	1.3759
20-30°	3.9335	1.3103
≤ 30°	4.4560	1.4843

4 Conclusion

This study presents an image-based metrology framework for efficient quality inspection of wide-area rebar placement structures, such as concrete walls. Unlike conventional inspection practices that rely on manual measurements, the proposed framework adopts a two-stage inspection pipeline integrating low-resolution region detection and high-resolution keypoint refinement using a Faster R-CNN, HRNet, and marker-based homography transformation. To support this framework, the Faster R-CNN detector was extended with a dual-head structure to jointly detect rebars and markers. A lightweight HRNet configuration was adopted for efficient high-resolution keypoint detection.

Experimental validation under varying distances and viewpoints demonstrated robust performance. The proposed method achieved 100% accuracy in identifying both vertical and horizontal rebars under all tested distances and viewing angles. The mean absolute error was 0.59 mm (3.53%) for diameter estimation and 4.05 mm (1.35%) for spacing estimation. These results fall within the permissible tolerance for rebar diameter estimation (0.8 mm) [9] and the commonly accepted error rate for rebar spacing estimation (10%) [10]. These results fall within permissible tolerances confirming stable and practical measurement performance.

Despite these promising results, several limitations remain. First, the experiments were conducted only in a controlled laboratory setting, while real construction sites may introduce complex visual conditions such as uneven lighting, shadows, and background clutter, affecting keypoint detection robustness. Second, the proposed framework requires manual installation of markers, which may introduce additional preparation time. Third, measurement errors may increase when the viewing angle exceeds approximately 30° due to the three-dimensional geometry of rebars, requiring careful camera positioning. Fourth, measurement accuracy may degrade at longer distances due to reduced image resolution.

Future work will address these limitations. First, real construction site data will be collected to evaluate the robustness and generalizability of the proposed method under diverse environmental conditions. Second, rebar-attached markers will be developed to reduce the time and complexity of marker installation. Third, marker-based algorithms will be developed to estimate viewing angles and provide real-time guidance for proper camera positioning in field conditions. Finally, approaches to improve effective pixel resolution at long distances will be investigated to enhance measurement accuracy.

Nevertheless, the proposed approach demonstrates the potential of a low-cost, image-based solution to support practical and scalable rebar quality inspection in the construction industry.

Acknowledgement

This research was funded by the National Research Foundation of Korea (NRF) grant funded by the Korean Government (Ministry of Science and ICT) (grant number RS202400356697).

References

[1] Y. Kardovskyi and S. Moon. Artificial intelligence quality inspection of steel bar installation by integrating Mask R-CNN and stereo vision. *Automation in Construction*, 130:103850, 2021.

[2] M. S. Shetty and A. K. Jain. *Concrete Technology: Theory and Practice*. S. Chand Publishing, New Delhi, India, 2019.

[3] Concrete Reinforcing Steel Institute (CRSI). *Placing Reinforcing Bars: Recommended Practices*, 9th ed. Concrete Reinforcing Steel Institute, Schaumburg, IL, USA, 2011.

[4] J. Song, H. Zhang, Y. Li, and J. Wang. An automatic rebar spacing measuring method based on the YOLOv8-GB model. *Measurement*, 242:116278, 2025

[5] M. K. Kim, J. P. P. Thedja, and Q. Wang. Automated dimensional quality assessment for formwork and rebar of reinforced concrete components using 3D point cloud data. *Automation in Construction*, 112:103077, 2020.

[6] X. Yuan, A. Smith, R. Sarlo, C. D. Lippitt, and F. Moreu. Automatic evaluation of rebar spacing and quality using LiDAR data: Field application for bridge structural assessment. *Automation in Construction*, 146:104708, 2023.

[7] A. H. Qureshi, W. S. Alaloul, A. Murtiyoso, S. J. Hussain, S. Saad, and M. A. Musarat. Smart rebar progress monitoring using 3D point cloud models. *Expert Systems with Applications*, 249:123562, 2024.

[8] X. Zhang, Y. Liu, J. Li, and H. Wang. A high-precision quality inspection system for steel bars based on machine vision. *Sensors*, 18(8):2732, 2018.

[9] W. Chen, X. Fu, W. Chen, and Z. Peng. Intelligent detection of rebar size and position using improved DeepLabV3+. *Applied Sciences*, 13(19):11094, 2023.

[10] U. Woo, M. Lee, T. Lee, H. Choi, S. M. Kang, and K. K. Choi. Real-time rebar spacing measurement system for quality control in construction. *Automation in Construction*, 171:106012, 2025.

[11] Y. G. Baek. Rebar inspection method using high-resolution image-based feature extraction and homography transformation. Master's Thesis, Hanyang University, Seoul, Republic of Korea. 2026.

[12] I. E. Bal, D. Dais, E. Smyrou, and V. Sarhosis. Novel invisible markers for monitoring cracks on masonry structures. *Construction and Building Materials*, 300:124013, 2021.

[13] A. Bakhtiarnia, Q. Zhang, and A. Iosifidis. Efficient high-resolution deep learning: A survey. *ACM Computing Surveys*, 56(7):1–38, 2024.